Ore Geology Reviews 133 (2021) 104057

Contents lists available at ScienceDirect

Ore Geology Reviews

journal homepage: www.elsevier.com/locate/oregeorev

Lithium and chlorine isotopic constraints on fluid sources and evolution at the Luziyuan distal skarn Zn–Pb–Fe–(Cu) deposit, western Yunnan Province, China

Lin Xu [a,b], Chongguang Luo [b,*], Hanjie Wen [a,b,c,*], Mingguo Deng [d,*], Chaojian Qin [b], Chuanwei Zhu [b], Jeffrey de Fourestier [a]

[a] State Key Laboratory of Nuclear Resources and Environment, East China University of Technology, Nanchang 330013, Jiangxi, PR China
[b] State Key Laboratory of Ore Deposit Geochemistry, Institute of Geochemistry, Chinese Academy of Sciences, Guiyang 550081, PR China
[c] University of Chinese Academy of Sciences, Beijing 100049, PR China
[d] Faculty of Land Resource Engineering, Kunming University of Science and Technology, Yunnan, Kunming 650093, PR China

ARTICLE INFO

Keywords:
Li isotopes
Cl isotopes
Skarn deposit
Rayleigh fractionation
Fluid-inclusion leachates
Luziyuan Zn–Pb–Fe–(Cu) deposit

ABSTRACT

The sources and temporal evolution of fluids related to distal skarn mineralization strongly influence the minerals that form, but remain poorly understood. In this study, we use the lithium and chlorine isotopic compositions of fluid-inclusion leachates (FIL) to elucidate the nature and evolution of fluids that formed the Luziyuan distal skarn Zn–Pb–Fe–(Cu) deposit, China. The δ^7Li values of prograde skarn stage rhodonite FIL (+5.37‰–+7.31‰) are similar to those of typical magmatic fluid. The δ^7Li values (+11.69‰–+12.54‰) of actinolite FIL are higher than those of rhodonite FIL; this is attributed to Rayleigh fractionation within a closed magmatic–hydrothermal system. It is inferred that up to 70% of fluid-borne Li is sequestered by hydrous minerals during retrograde skarn alteration, consistent with conclusions drawn from previous studies of fluid-inclusions. The δ^7Li values of galena FIL (+9.78‰–+13.19‰), black sphalerite FIL (+11.62‰), and reddish-brown sphalerite (+10.44‰–+11.66‰) overlap with those of actinolite FIL, indicating that phase separation occurred during Zn–Pb mineralization at the Luziyuan deposit. The low δ^7Li values of light-yellow sphalerite FIL (+6.75‰) and calcite FIL (+3.95‰–+6.49‰) record external fluid input, probably meteoric water. The positive δ^{37}Cl values of rhodonite FIL (+1.82‰–+1.83‰) are consistent with those of magmatic fluids. However, the δ^{37}Cl values of actinolite FIL (+0.49‰) are lower than those of rhodonite FIL, indicating that FIL within hydrous minerals might not record fluid sources reliably.

1. Introduction

Lithium (Li) isotopes have been used to investigate the sources of brines, formation fluids, and geothermal fluids (e.g., Chan et al., 2002; Millot et al., 2010a, 2010b), subduction-related dehydration (e.g., Zack et al., 2003; Marschall et al., 2007; Romer and Meixner, 2014), and hydration and weathering of oceanic crust (e.g., Foustoukos et al., 2004; Millot et al., 2010b; Barnes and Cisneros, 2012), as it is a fluid mobile light element and the isotopic fractionation is relatively large during fluid-related processes that redistribute elements. Lithium isotopes do not fractionate to a measurable degree at high temperatures (>1000 °C) during differentiation of basaltic magmas (Tomascak et al., 1999). However, fractionation of Li isotopes during evolution of granitic magma, and amongst minerals and coexisting fluids at 500–900 °C has been reported (Teng et al., 2004, 2006, 2009, Wunder et al., 2006, 2007, 2010; Bryant et al., 2004; Magna et al., 2010). These findings indicate that the Li isotopic fractionations might be a valuable indicator of the mineralization, including Zn–Pb mineralization, where temperatures are typically <400 °C. Recent studies have shown that Li isotopic composition of fluid inclusions has great potential to provide insights into the sources, evolution, and mixing of ore-forming fluids (Masukawa et al., 2013; Yang et al., 2015; Richard et al., 2018; Xu et al., 2018). Lithium, as well as the Pb and Zn that are of interest in the present study, are commonly transported by Cl-bearing species, so Li isotopes are

* Corresponding authors at: State Key Laboratory of Nuclear Resources and Environment, East China University of Technology, Nanchang 330013, Jiangxi, PR China (H. Wen).
E-mail addresses: luochongguang@vip.gyig.ac.cn (C. Luo), wenhanjie@vip.gyig.ac.cn (H. Wen), mingguod@163.com (M. Deng).

https://doi.org/10.1016/j.oregeorev.2021.104057
Received 21 October 2020; Received in revised form 4 February 2021; Accepted 7 February 2021
Available online 16 February 2021

expected to constrain the source and evolution of the ore-forming fluid.

Anions (e.g., F^-, Cl^-, SO_4^{2-}, S^{2-}) govern the solubility and mobility of ore-forming metals in magmatic systems and brine systems (Wood and Samson, 1998). Of these, Cl is the most important in ore-forming fluids, because most metals (e.g., Zn, Pb, Cu, Sn) are thought be transported by Cl-complexes (Yardley, 2005). Chlorine partitions strongly into fluids during fluid-rock interaction. The Cl isotopic composition of fluid-inclusion leachates (FIL) is widely used to identify sources of salinity in ore-forming fluids (e.g., evaporated seawater, halite solubility, magma) in rare- and base-metal deposits (e.g., Eastoe et al., 1989; Banks et al., 2000a, 2000b, 2002; Richard et al., 2011; Andersson et al., 2019).

Distal skarn Zn–Pb deposits are commonly thought to form from complex metamorphism amongst carbonate rocks and hydrothermal fluids, and mineralizing fluids are thought to migrate over long distances (e.g., Meinert et al., 2005; Samson et al., 2008). The fluid sources usually remain controversial, particularly in the deposits without igneous rocks in the vicinity. Magmatic hydrothermal fluids have been recognized as major fluid sources of the prograde alteration stage to produce anhydrous skarn (e.g., Meinert et al., 2005; Palinkas et al., 2013; Vezzoni et al., 2016), whereas magmatic and/or meteoric fluids are identified during the retrograde skarn hydrous stage (Palinkas et al., 2013). However, the temporal evolution of ore-forming fluids is poorly documented (Shu et al., 2017). The Luziyuan skarn Zn–Pb–Fe–(Cu) deposit in Yunnan Province provides an excellent opportunity to investigate the nature and evolution of fluids that are responsible for skarn Zn–Pb mineralization. This deposit has been mined for over 50 years, and contains approximately 280 Mt of Zn + Pb ore at 5.09% Zn and 2.40% Pb and 301 Mt of Fe ore at 30.02% TFe (Deng et al., 2016, 2018; Xu et al., 2019). The paragenesis of Zn–Pb mineralization at this deposit has been studied extensively (Liu and Deng, 2014; Deng et al., 2018; Xu et al., 2019). Moreover, primary fluid inclusions are common within minerals that formed throughout the evolution of the deposit, so the Li and Cl isotopic compositions of FIL can be analyzed by crush–leach techniques.

In this study, we first present data on lithium and chlorine isotopes in fluid inclusions in gangue minerals and ore minerals formed during all stages of mineralization and alteration at the Luziyuan deposit. We discuss the origin of ore-forming fluids, fluid–rock reaction, and mineral precipitation, and summarize the temporal changes in the Li and Cl isotopic compositions of fluids as the ore-forming system evolved.

2. Geological setting

The Baoshan Block is the northern extension of the Sibumasu Block, and is bounded by the Changning-Menglian suture to the east and the Gaoligong fault to the west (Fig. 1, Sone and Metcalfe, 2008). Closure of the Tethys Ocean and collision between the Indian and Eurasian plates caused orogenesis, and continental collision compressed the Baoshan Block into a wedge shape, forming numerous strike-slip faults within the block (Deng et al., 2014a).

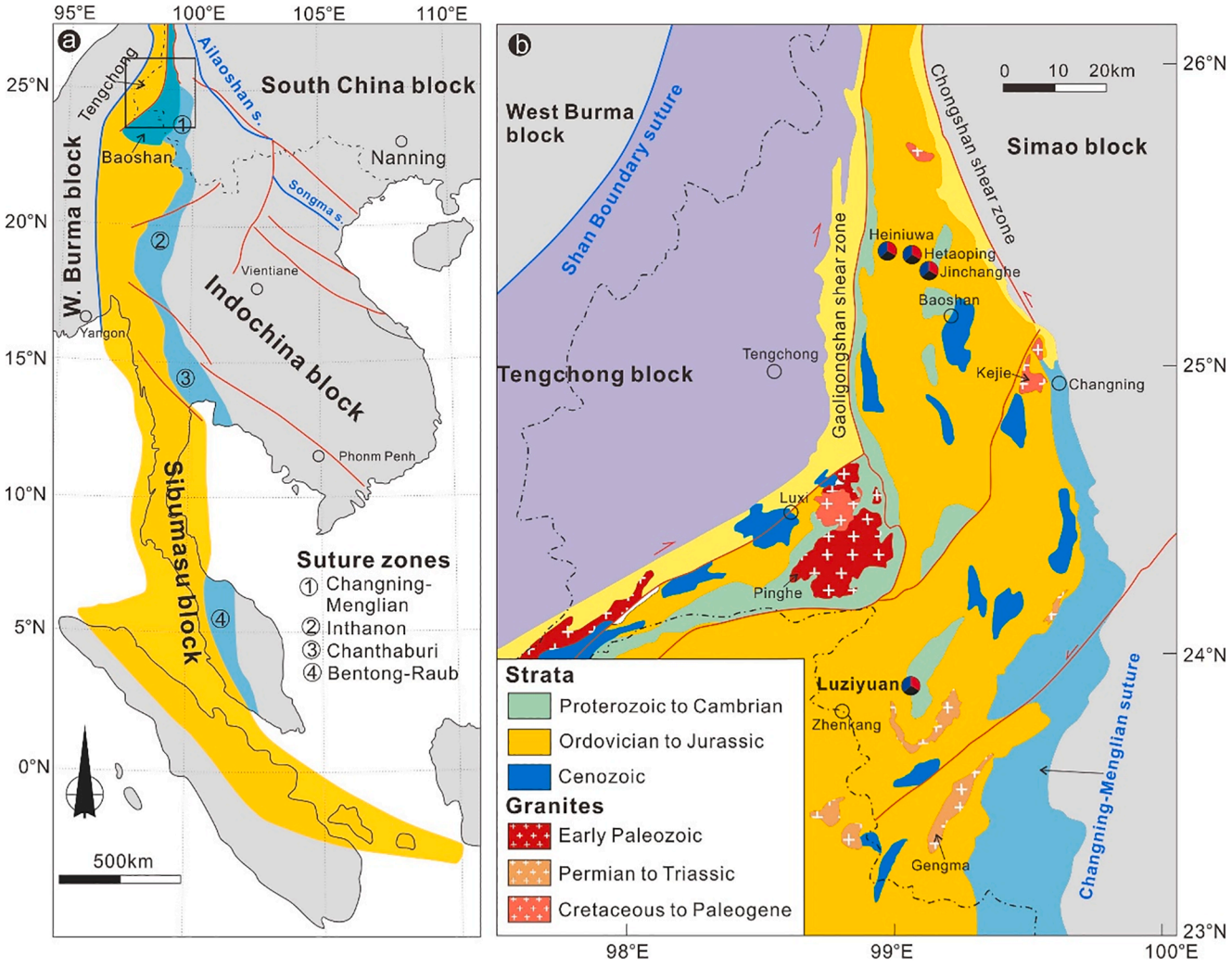

Fig. 1. (a) Simplified geological map of the Sibumasu Block and adjacent regions (modified from Sone and Metcalfe, 2008). (b) Geological map showing the regional tectonic framework of the Baoshan Block, distribution of sedimentary and igneous units, and major skarn Zn–Pb deposits (modified from Deng et al., 2014a).

The Gongyanghe Group forms the basement of the Baoshan Block, and comprises the late Neoproterozoic to the Cambrian weakly metamorphosed siliciclastic and carbonate rocks, which are locally intercalated basic volcanic rocks with minor ca. 499 Ma (zircon U–Pb age) (Yang et al., 2012). The basement is unconformably overlain by the Paleozoic to Mesozoic sedimentary strata, and minor Permian volcanic rocks. The sedimentary rocks are dominated by a set of neritic to shore carbonates, sandy shale and clastic rocks. The Paleozoic carbonates host major skarn-type Zn–Pb deposits, such as the Luziyuan, Hetaoping and Jinchanghe deposits (Tao et al., 2010; Deng et al., 2014a, 2018; Chen et al., 2017).

Early Paleozoic and Mesozoic–Cenozoic granitoids intruded the Baoshan Block during a number of intermediate–silicic magmatic events. Early Paleozoic granitoids with zircon U–Pb ages of 500–450 Ma crop out mainly within the Pinghe, Mengmao, and Shuangmaidi areas (Liu et al., 2009; Dong et al., 2013). The Middle Permian to Triassic alkali granites related to collision between the Baoshan and Simao blocks, such as the Muchang and Gengma plutons, occur close to the eastern and southern margins of the Baoshan Block. The Cretaceous S-type granites include the Zhibenshan, Gaoligong and Kejie plutons, and have yielded ages of 126.7 ± 1.6 Ma, 126–118 Ma and 93 ± 13 Ma, respectively (Yang et al., 2006; Tao et al., 2010). These granites are thought to be the products as a consequence of the melting of thickened crust during closure of the Neo-Tethys Ocean (Yang et al., 2006; Tao et al., 2010). The distal skarn mineralization in the Baoshan Block is considered to potentially have a genetic link with the Cretaceous intermediate-felsic magmatism. The calcite Sm–Nd method has yielded ages indicating that the Luziyuan formed at 130 ± 15 Ma (Xu et al., 2020).

3. Deposit geology

The Luziyuan deposit is one of the best-documented distal skarn Zn–Pb deposits in the Baoshan Block (Fig. 2). Only Cambrian strata, dominated by limestone, marble and minor calcic slate, are present in the Luziyuan district. The Medium Cambrian Shahechang Formation (Member 2 and 3) is principal host rock of the orebodies, and consists of marble, argillaceous limestone, silty slate, minor chlorite skarn and diabase dykes (Deng et al., 2014b, 2018). Sparse diabase dikes that yield an age of 362 ± 1.5 Ma occur close to NE–SW-trending faults (Deng et al., 2018). The strata are strongly deformed and form a kilometer-scale anticline referred to as the Luziyuan inverted anticline. The anticlinal core is cut by sets of NE- and NW-trending faults (Fig. 2a). The former is mainly composed of extensional shear (e.g., F1, F2, F3, F4, and F5) (e.g., Yang and Luo, 2011; YGS, 2012), while the latter primarily consists of compressional shear (e.g., F6, F7, F8, F9, F12, and F13) (Xia et al., 2005; YGS, 2012). The emplacement of Zn–Pb and Fe orebodies is structurally controlled by the NE-trending faults.

Intense skarn alteration is widespread within the Luziyuan district, and is closely associated with Zn–Pb–Fe–(Cu) mineralization. Sphalerite, galena and magnetite usually coexist in the skarn alteration zone, and form densely disseminated, vein and massive skarn ores. The main ore minerals are sphalerite, galena, magnetite, pyrite, chalcopyrite, with minor bornite, pyrrhotite, arsenopyrite and chalcocite. The main gangue minerals are rhodonite, actinolite, chlorite, andradite, quartz, and calcite. Additionally, silicic and carbonate alterations primarily consist

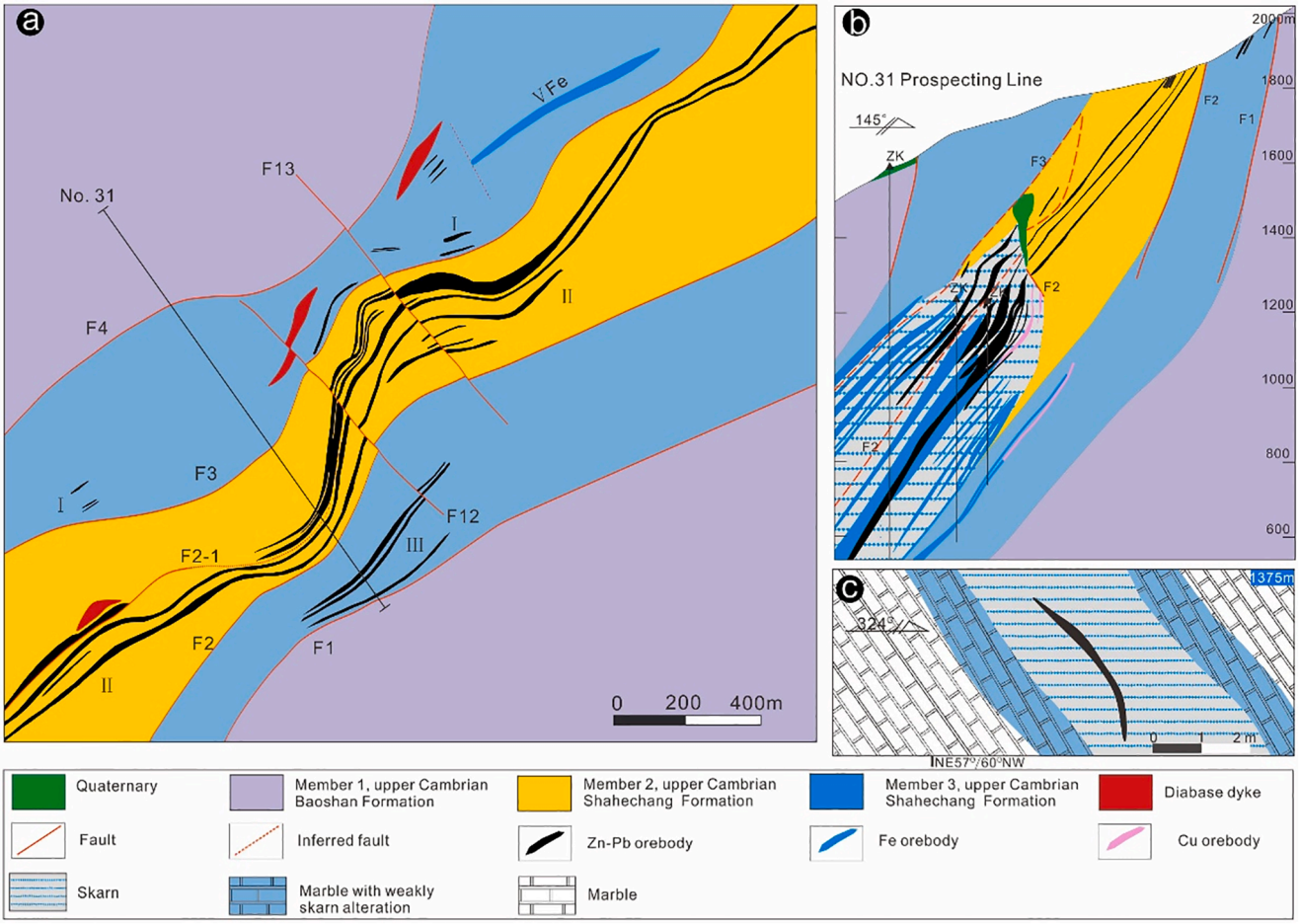

Fig. 2. (a) Geological map of the Luziyuan skarn deposit, modified from Deng et al. (2018). (b) Geological cross-section along prospecting line No. 31 at the Luziyuan skarn deposit, modified from Xu et al. (2019). (c) Geological cross-section at 1375 m on prospecting line No. 27.

of quartz and calcite, respectively, which commonly overprint the earlier skarn.

The Luziyuan deposit comprises four ore bodies: Zn–Pb ore bodies Nos. I, II, and III, and the No. V Fe ore body. These orebodies mainly occur as lenticular and stratabound veins in shape (Fig. 2a). The ore metals display a zonation of Fe–Cu, Fe–Cu–Zn–Pb and Zn–Pb in a vertical direction from the deep skarn to the shallow marble (Fig. 2b). The largest orebody – No. II has a Zn grade of 2.95%–3.14%, Pb 0.30%–0.55%, and TFe with 17.90%–29.49%. It strikes 285°–345° NE and 32°–78° NW with approximately 3000 m in length and 7–20 m in width.

Four main stages of alteration and mineralization are recognized at the Luziyuan deposit, based on extensive textural and mineralogical observations (Zeng et al., 2014; Deng et al., 2018; Xu et al., 2019): (1) Prograde skarn alteration stage; (2) Retrograde skarn alteration stage; (3) Sulfide ore stage; and (4) Post-ore stage. Garnet, pyroxene, and pyroxenoids are typical of the earliest prograde alteration. Garnet is typically pinkish-red to crimson, euhedral–subhedral, and fine-grained (<1.5 mm). In some case, garnet displays a crushed or relict texture under the microscope, and is partly to completely replaced by actinolite, epidote and chlorite (Zeng et al., 2014; Xu et al., 2019). The garnets are classified as the andradite–grossular series, with a compositional range of $Ad_{61\text{-}84}Gr_{3\text{-}22}Py_{13\text{-}17}$ (Zeng et al., 2014). Pyroxene is mostly fibrous and radiating, stubby–prismatic, or striated and bladed. Minor lamellar of pyroxene are intergrown with the pyroxenoids. Pyroxenes are members of the diopside–johannsenite–hedenbergite series, with an average composition of $Di_{47}Jhn_{32}Hd_{21}$ (Zeng et al., 2014). Pyroxenoids are the most common prograde mineral at the Luziyuan deposit (Deng et al., 2014b), and rhodonite is the most common pyroxenoid (Zeng et al., 2014). Rhodonite is typically pink–red, anhedral, and coarse-grained. It commonly occurs as massive aggregates within units of residual host rock on the middle–lower levels of the deposit (<1500 m). Rhodonite is typically surrounded by retrograde hydrous silicates, such as actinolite and epidote.

The retrograde skarn alteration stage is characterized by large amounts of actinolite, chlorite, and epidote, with minor quartz and fluorite. This alteration is related to Fe mineralization. Actinolite typically coexists with chlorite and occurs as stumpy and radiating fibrous massive aggregates within the host marble. Most of the magnetite occurs deep within the mine as bands or veinlets within the skarn, and is commonly interstitial to, or replaces, garnet. Quartz and calcite occur as veins, and are interstitial to, or replace, prograde skarn minerals.

The sulfide ore stage is characterized by large amounts of sulfides, such as sphalerite, galena, pyrite, arsenopyrite, chalcopyrite, and bornite. Euhedral coarse-grained pyrite is the earliest sulfide mineral, and is commonly replaced by sphalerite, galena, and chalcopyrite. Sphalerite and galena are the main ore minerals. Sphalerite is typically black- to light-yellow, euhedral–subhedral, coarse-grained, and closely associated with galena. Sphalerite also occurs interstitial to actinolite within the skarn. Minor amounts of chalcopyrite are present in many samples. The sulfide-rich mineral assemblages form disseminated ore, banded ore, massive ore, and veins or stockwork that cross-cut or fill gaps within the skarn minerals. Massive ore commonly coexists with quartz and calcite in large cracks between the skarn and marble. Post-ore stage minerals include calcite, quartz, and fluorite, which form late veins that cross-cut the earlier assemblages.

4. Samples and methodology

4.1. Samples

We mainly collected samples from 1375 m sub-level in this deposit, where ore bearing veins predominantly occur in the skarn alteration zone. Fig. 2c demonstrates the characteristic skarn alteration and mineralization from the central to both boundaries in the sub-level: the central part of skarn alteration zone is primarily composed of rhodonite, actinolite and chlorite with minor irregular sulfide veins (sphalerite and galena) infilled in the cracks of these skarn minerals.

Weak skarn alteration appears in the marble in the contact zones. It is characterized by the occurrence of minor hydrous silicate (chlorite and epidote) with locally lamellar or spotted sulfides. To characterize the signatures on Li and Cl isotopic compositions during the ore-forming process, we selected representative minerals for subsequent crush-leach method of analysis from all the mentioned stages (Figs. 3 and 4). These included five prograde-stage rhodonite samples, five retrograde-stage actinolite samples, five ore-stage sphalerite samples (black, reddish-brown and yellow), three ore-stage galena samples, and six post-stage calcite samples.

4.2. Extraction of fluid-inclusion leachates

Block specimens were crushed using a metal ramming bowl and screened to a grain size of 20–40 mesh, and then grains were hand-picked for purity under a binocular microscope until amounts of 1–3.5 g were obtained. Next, the picked mineral grains were cleaned ultrasonically and dried in a baking oven. The weighed samples were crushed and leached by a planetary ball mill equipped with four agate cups, filled with 35 mL ultrapure water, at high-speed rotation for about 40 mins, which was sufficient for the complete release of fluid inclusions into the water. Finally, the leachates were transferred to a suitable container and passed through 0.2 μm nylon filters to remove particulates before analysis.

4.3. Composition of the leachates

The analysis of the leachates was performed at the State Key Laboratory of Environment Geochemistry, Institute of Geochemistry, Chinese Academy of Sciences. The Cl concentration was measured by a Dionex ICS-90 ion chromatograph, with a detection limit of < 0.01 mg L^{-1}. The Li and Sr concentrations were analyzed by inductively coupled plasma–mass spectroscopy (ICP–MS) on a NexION 300X instrument. The detection limit was < 0.01 μg L^{-1}. Uncertainties on all element concentrations are < 10% relative.

4.4. Lithium isotope measurements

Chemical procedures and determination of Li isotopes were performed at the State Key Laboratory of Ore Deposit Geochemistry, Institute of Geochemistry, Chinese Academy of Sciences. A two-step column chemistry was employed to isolate Li from the sample matrix. Details are described in Xu et al. (2020a), Xu et al. (2020b). Sample solutions first passed through a column loaded with 7 mL of Dowex 50WX8 (200–400 mesh) resin for the removal of most matrix elements. Residual Na in samples was further eliminated through another column loaded with 2.5 mL of the resin. The collected solutions were dried at 120 °C, and then the residue was dissolved in 2% v/v HNO_3 for subsequent isotope ratio analysis.

Purified solutions containing 50 μg L^{-1}Li were introduced to Ar plasma through a PFA nebulizer. Li isotopes ratios were obtained using the standard–sample bracketing (SSB) protocol in a Neptune MC–ICP–MS. $^6Li^+$ and $^7Li^+$ were simultaneously collected in a low-mass Faraday cup (L4) and a high-mass cup (H4), respectively. Intensity of the ion current was approximately 1.3 A for 50 μg L^{-1} standard solution, much higher than background Li signal ($<10^{-4}$ V). All data were reported in per mil relative to IRMM-016. To monitor the isotopic fractionation during the chemical pre-treatment, seawater (CASS-5; National Research Council of Canada), rock references (BCR-2) and Li isotopes standard solution (IRMM-016) were treated as unknown samples. The results yielded δ^7Li values of +30.91‰ ± 0.16‰ for CASS-5, +2.69‰ ± 0.31‰ for BCR-2 and −0.01‰ ± 0.17‰ for IRMM-016, consistent with published values (e.g., Tomascak et al., 1999; Tian et al., 2017; Xu et al., 2018, 2020a, 2020b; He et al., 2019).

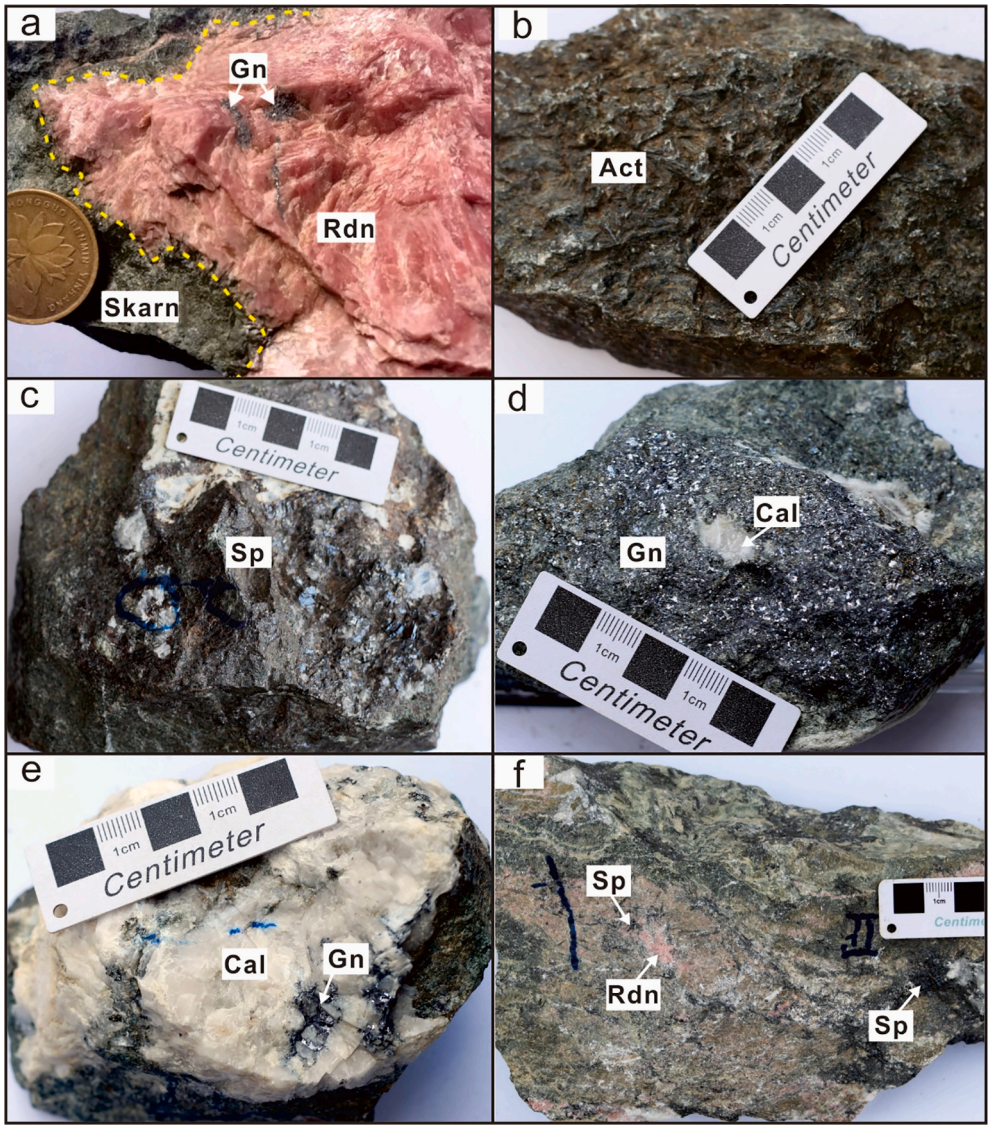

Fig. 3. Photographs of hand specimens. (a) Massive rhodonite and fine galena veins. (b) Radiating and fibrous actinolite. (c, d) Typical ore assemblage consisting mainly of sphalerite and galena. (e) Post-ore stage calcite veins containing fine galena veins. (f) Disseminated sphalerite with rhodonite and chlorite. Abbreviations: Rdn = rhodonite; Act = actinolite; Sp = sphalerite; Gn = galena; Cal = calcite.

4.5. Chlorine isotope measurements

Sample preparation for the determination of Cl isotopes was modified from the procedures described by Luo et al. (2012), Luo et al. (2014). Before being treated through column processes, all solutions were concentrated in 50–100 μL to 7 mL Teflon breakers. H- and Cs-form resin column (both infilled with 0.2 mL resin) were consecutively connected to achieve the conversion of CsCl. Relevant reactions in the column process are $H^+ + Cl^- \rightarrow HCl$ for the former and $Cs^+ + HCl \rightarrow CsCl + H^+$ for the latter. A pH test strip was used to check if the conversion succeeded. A minimum of 50 μg of Cl for each sample was processed using the above chemical procedures. The obtained CsCl solutions were concentrated to 20–30 μL at a temperature range of 40–60 °C for subsequent isotope ratio measurement.

The $^{37}Cl/^{35}Cl$ ratio was measured through positive thermal ionization mass spectrometry (P-TIMS) based on graphite loaded Cs_2Cl^+, at the Qinghai Institute of Salt Lakes, Chinese Academy of Sciences. A preparation of 2.5 μL graphite slurry in 80% ethanol and 3 μL test solutions was successively loaded on the central of outgassed Ta filament and dried using a current of 1 A for 1.5 min in a clean air flow unit. The prepared sample disk was then placed in the ion source of the mass spectrometer. Isotope ratio analysis was begun once the ion source was under of a vacuum of $<2.5 \times 10^{-7}$ mbar. Intensity of the Cs_2Cl^+ ion was adjusted to 4×10^{-12} A by controlling the filament current. The isotopic data were simultaneously obtained on Faraday cup C and H1 by collecting the ion flow with mass numbers of 301 ($^{133}Cs_2^{35}Cl^+$) and 303 ($^{133}Cs_2^{37}Cl^+$), respectively. All data were reported in per mil delta notation relative to ISL 354. Repeated analysis of Cl isotopes standard (ISL 354 NaCl) yielded an average $^{37}Cl/^{35}Cl$ ratio of 0.319030 ± 0.000071 (2σ).

5. Results

Leachate compositions are provided in Table S1, and the Li and Cl isotopic compositions and Li concentrations of analyzed minerals and marble are provided in Tables 1 and 2, respectively. The δ^7Li values of rhodonite FIL and retrograde-stage actinolite FIL range from + 5.37‰ to + 7.91‰, with an average of + 6.69‰ ($n = 5$), and + 11.69‰ to + 12.54‰ ($n = 5$), respectively (Table 1). The δ^7Li value of black sphalerite FIL (+11.62‰, $n = 1$) is similar to that of reddish-brown sphalerite FIL (+10.44‰–+11.66‰, $n = 3$), but higher than that of light-yellow sphalerite FIL (+6.75‰, $n = 1$). The δ^7Li values of galena FIL are +

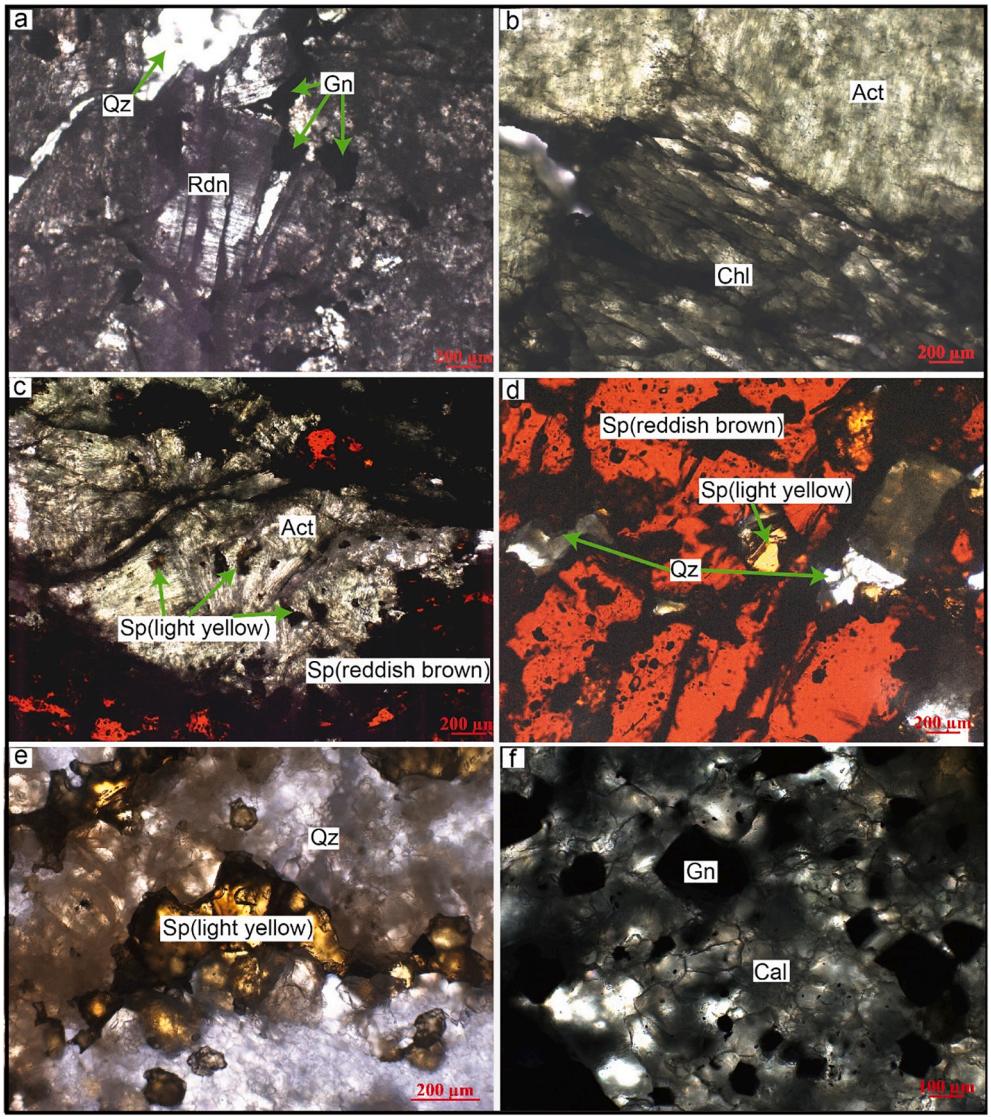

Fig. 4. Photomicrographs showing textures. (a) Irregular galena interstitial to skarn rhodonite. (b) Intergrown actinolite and chlorite. (c) Reddish-brown sphalerite amongst spiculate actinolite aggregates. (d) Reddish-brown sphalerite with inclusions of light-yellow subhedral sphalerite and quartz. (e) Light-yellow sphalerite cutting quartz vein. (f) Interstitial inclusions of galena in calcite. Abbreviations: Rdn = rhodonite; Act = actinolite; Gn = galena; Sp = sphalerite; Qz = quartz; Cal = calcite.

9.78‰–+13.19‰ (n = 3). The δ^7Li values of calcite FIL are the lowest, and range from + 3.95‰ to + 6.49‰ (n = 6). The Li contents of rhodonite (1.04–2.30 μg g^{-1}), actinolite (11.10–18.75 μg g^{-1}), sphalerite (0.30–3.76 μg g^{-1}), and calcite (2.40 μg g^{-1}) are shown in Table 2 and Fig. 5a. The Li isotopic compositions of minerals are strongly related to those of the corresponding leachates. Actinolite has the highest δ^7Li value (+1.71‰), followed by sphalerite (-3.68‰), calcite (−4.73‰), and rhodonite (-5.97‰) (Fig. 5b). The marble (mbl) sample contains only 1.03 μg g^{-1}Li and possesses a δ^7Li value of −3.32‰, which provides the estimation of δ^7Li value of pristine marble at the Luziyuan deposit.

The δ^{37}Cl values of rhodonite FIL are positive (+1.83‰–+1.85‰, n = 2). The δ^{37}Cl value of actinolite FIL is lower (+0.49‰, n = 1), and slightly higher than that of seawater (0‰).

6. Discussion

6.1. Lithium isotopes

Fluid inclusion leachates from the Luziyuan deposit have variable δ^7Li values (+3.95‰–+13.19‰) that are higher than those of typical magmatic fluids (−4‰–+4‰) (Masukawa et al., 2013; Richard et al., 2018) (Fig. 6a). This might be indicative of origin of the ore-forming fluids and later processes involving lithium isotopic fractionation, such as fluid exsolution, contribution from country rock, and skarn alteration.

Lithium is preferentially distributed into the fluid phase under the equilibrium condition (770–900 °C, 0.5–2.0 kbars) between granitic melts and aqueous fluid (Webster et al., 1989). If the extent of fractionation during fluid exsolution is known, then the Li isotopic composition of the magmatic fluid source can be estimated. Calculations show that exsolution of supercritical fluids from granitic melts by Rayleigh distillation is associated with minor fractionation of Li isotopes (Teng et al., 2006). Moreover, Yang et al. (2015) measured Li isotopic compositions of quartz FIL and andesite from the Gacun VMS Zn–Pb deposit. They found that the minimal value (+4.5‰) of FIL representing initial magmatic fluids and agrees well with the andesite (+1‰–+2‰), suggesting a magmatic origin for the deposit. Based on this, fractionation during fluid exsolution might induce differences in δ^7Li values of up to 3‰, agreeing well with empirical studies (Chan et al., 1994; Teng et al., 2006; Wunder et al., 2006). Therefore, it is reasonable to deduce that most of the magma-derived Li might be partitioned in fluids, and those fluids might have similar Li isotopic compositions to the crystallized peraluminous rock. In addition, the low Li content (0.17 μg g^{-1}) and δ^7Li value (−3.2‰) in marble at the Luziyuan deposit indicate the country rock could not account for isotopically heavier Li of the ore-forming

Table 1
Fluid inclusion leachate δ^7Li values and δ^{37}Cl values.

Sample		δ^7Li (‰)	2σ	δ^{37}Cl (‰)	2σ	Mineral assemblage	Note
LZY-NO24	Rdn FIL	+6.88	0.08			Rdn + Act + Bn	
LZY-NO13-2	Rdn FIL	+6.17	0.07	+1.85	0.00	Rdn + Sp + Gn	
LZY-NO27	Rdn FIL	+7.91	0.40			Rdn + Act + Sp	
LZY-NO29	Rdn FIL	+7.12	0.09			Rdn + Act + Sp	
LZY-NO30	Rdn FIL	+5.37	0.01	+1.83	0.22	Rdn + Act + Chl	
LZY-NO12	Act FIL	–	–			Act + Chl	
LZY-NO20	Act FIL	+12.54	0.34			Act + Chl + Apy	
LZY-NO24	Act FIL	+11.48	0.14			Rdn + Act + Bn	
LZY-NO30	Act FIL	+11.69	0.14	+0.49	0.13	Rdn + Act + Chl	
LZY-NO28	Act FIL	+12.04	0.34			Act + Chl + Sp	
LZY-NO9-2	Sp FIL	+11.62	0.42			Sp + Gn + Qz	Black Sp
LZY-NO32	Sp FIL	+10.44	0.15			Chl + Sp + Cal	Reddish brown Sp
LZY-NO6	Sp FIL	+11.66	0.18			Chl + Sp + Cal	Reddish brown Sp
LZY-NO33	Sp FIL	+11.02	0.08			Chl + Sp + Cal	Reddish brown Sp
LZY-NO11	Sp FIL	+6.75	0.49			Rdn + Act + Sp + Gn	Light yellow Sp
LZY-NO15	Gn FIL	+10.55	0.10			Gn + Cal	
LZY-NO9-2	Gn FIL	+9.78	0.76			Sp + Gn + Qz	
LZY-NO5	Gn FIL	+13.19	0.40			Sp + Gn + Qz	
LZY-NO3	Cal FIL	+6.49	0.35			Bn + Cal	
LZY-NO4-1	Cal FIL	+3.95	0.35			Chl + Gn + Cal	
LZY-NO4-2	Cal FIL	+4.04	0.37			Chl + Gn + Cal	
LZY-NO7-1	Cal FIL	+5.43	0.67			Sp + Cal + Qz	
LZY-NO7-2	Cal FIL	+5.42	0.36			Sp + Cal + Qz	
Sample		δ^7Li (‰)	2σ	δ^{37}Cl (‰)	2σ	Mineral assemblage	Note
LZY-NO8	Cal FIL	+5.67	0.52			Sp+Gn+Cal	
BCR-2		+2.69	0.31				Basalt standard
CASS-5		+30.91	0.16				Seawater
IRMM-016		+0.01	0.17				Pure Li

Abbreviations: Rhn = Rhodonite; Act = actinolite; Chl = chlorite; Sp = sphalerite; Gn = galena; Apy = arsenopyrite; Bn = bornite.

Table 2
Mineral and host rock Li concentrations and isotopic compositions.

Sample	Mineral/rock	Li content	δ^7Li (‰)	2SD
LZY-NO27	Rdn	1.04	−5.97	0.07
LZY-NO30	Act	11.10	+1.71	0.39
LZY-NO6	Sp	3.76	−3.7	0.03
LZY-NO3	Cal	2.41	−4.7	0.05
M1	Marble	0.17	−3.32	0.48

fluids during the skarn alteration. These considerations show conclusively that the slightly high δ^7Li values (+5.37‰–+7.91‰) of rhodonite FIL, relative to those reported for magmatic fluids, reflect the Li isotopic composition of the intermediate–silicic magma that provided the fluids.

The Cretaceous granite in the Baoshan and Tengchong block, associated with the abundant skarn Zn–Pb deposits, are known to originate from partial melting of the Archean–Proterozoic lower crust during subduction of the Meso- and Neo-Tethys oceanic plate (Deng et al., 2014a). Previous studies concluded that this crust has high δ^7Li values (Magna et al., 2016; Teng et al., 2008; Tian et al., 2017; Wang et al., 2019). For instance, Magna et al. (2016) found >+10‰ δ^7Li values in a global compilation of Archean pegmatites related to continental crust growth. Therefore, we suggest that the lithium isotopic characteristics of ore-forming fluids during the prograde skarn alteration might be inherited from the Cretaceous granitic magma within the Baoshan Block.

Compared to rhodonite FIL, actinolite FIL are found to have significant higher δ^7Li values (+11.69‰–+12.54‰) (Fig. 6b). Predominant magmatic features are also recorded in the retrograde skarn alteration stage at the Luziyuan deposit, based on the published H–O isotopes data (Deng et al., 2018; Xu et al., 2019). This suggests that the heavy isotopic Li tends to reflect the factor controlling the variation of δ^7Li values within a framework of temporal fluid evolution in a closed system, rather than addition of Li from a different reservoir. The prograde (233.6–315.6 °C) and retrograde (214.9–388.0 °C) skarn stages have similar temperatures (Deng et al., 2018), so temperature was not the main control on Li isotope fractionation, but Rayleigh fractionation might have caused variation in the δ^7Li values.

It is suggested that partition coefficient of Li between fluid and minerals (Kmin/fluid p(Li)) covered a large range of 0.0004 to 152 (Brenan et al., 1998; Caciagli et al., 2011; Fabbrizio et al., 2013). Anhydrous minerals such as olivine, clinopyroxene, and garnet have the lowest Kmin/fluid p(Li)(<0.3) values. Hydrous minerals that form by aqueous alteration, such as amphibole, epidote, and serpentine, have high Kmin/fluid p(Li)values; the Kmin/fluid p(Li)value for amphibole at 2 GPa and 900 °C is 0.82, and the Kmin/fluid p(Li)value for chlorite at 260 °C is 2.6 (Berger et al., 1988; Fabbrizio et al., 2013). Berger et al. (1988) inferred an increase in Kmin/fluid p(Li)values for hydrous minerals with decreasing temperature. In addition, lithium partition has an affinity for minerals containing volatile components (B, Cl, F) (Webster et al., 1989; Teng et al., 2006). Higher Kmin/fluid p(Li) between hydrous minerals and fluids would be expected during the retrograde skarn alteration at the Luziyuan, where the temperature is obviously lower than those reported by Fabbrizio et al. (2013). Therefore, Li is retained by ore-forming fluids during prograde skarn alteration, but is compatible during retrograde skarn alteration.

At the Luziyuan deposit, formation of actinolite, chlorite and mica during the retrograde skarn alteration stage is prone to extract a large amount of Li from the ore-forming fluids (Table 2, Fig. 5), which results in the fractionation. Lithium commonly occupies octahedral coordination in most silicate minerals (e.g., garnet, olivine, pyroxene) through substitution for Mg (e.g., Shannon, 1976; Wenger and Armbruster, 1991), whereas it enters a lower coordinated site (3.2 to 5 (generally 4), depending on fluid density) in aqueous fluids (Jahn and Wunder, 2009). Since the lighter isotope preferentially occupies the more highly coordinated site, ^{7}Li is preferentially partitioned into aqueous fluids (Wunder et al., 2006, 2007, 2010).

Rayleigh fractionation calculations were performed to simulate Li removal from fluids with an initial δ^7Li value of +6.69‰, based on rhodonite FIL from the Luziyuan deposit (Fig. 7). Their fractionation factors (α, where α = (^{7}Li/^{6}Li) mineral /(^{7}Li/^{6}Li) fluid) were calculated from an expression based on the experiments of Wunder et al. (2006):

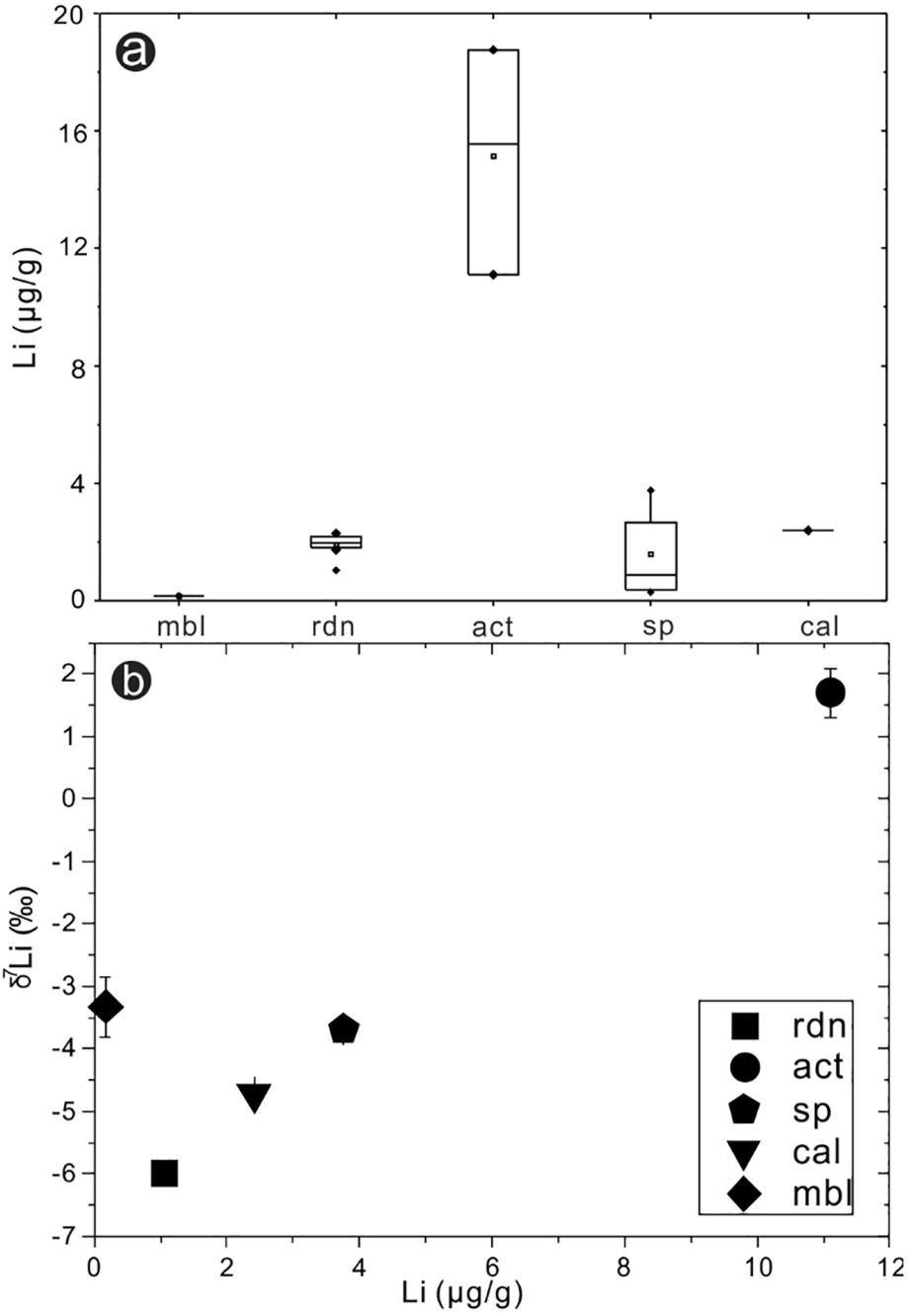

Fig. 5. (a) Lithium concentrations of host rock and minerals. Some of the data are from Deng et al. (2016). (b) δ^7Li values versus Li concentrations.

$\alpha_{(\text{mineral–fluid})} = 4.61 \times (1000/T) + 2.48$ ($R^2 = 0.86$), where T is temperature. Calculated values of α range from 0.994 at 275 °C to 0.997 at 500 °C. The experiments were conducted between 500 °C and 900 °C, but the calculated α is in good agreement with the measured fractionation between hot spring water and altered basalt at a lower temperature (350 °C) (Chan et al., 1993). At previously established homogenization temperatures for fluid inclusions formed during prograde and retrograde skarn alteration (Deng et al., 2018), 60%–70% Li is expected to be removed from the fluids as a consequence of Li uptake in the hydrous minerals (Fig. 8), which corresponds to an increase of about +6‰ δ^7Li values in actinolite FIL. Such an estimation is supported by the significantly decreasing Li content in fluid inclusions from the prograde to retrograde skarn stages at other skarn Zn–Pb deposits, based on LA–ICP–MS data (Shu et al., 2017).

The above model prediction is also consistent with the mentioned Li partition and heavy δ^7Li value in actinolite (Fig. 5). The δ^7Li values of FIL are higher than those of their host minerals (Fig. 8), consistent with the low Li coordination numbers in aqueous fluids inferred by experimental and theoretical studies (Jahn and Wunder, 2009; Wunder et al., 2006). From a Rayleigh fractionation perspective, assuming that Li in the later-formed minerals is mainly from earlier stage fluids in a closed system, the later-formed minerals would be expected to have higher δ^7Li values than the earlier-formed minerals. This trend is consistent with the difference in δ^7Li values between rhodonite (LZY-NO27) and actinolite (LZY-NO30) (Fig. 8). Consequently, most of the Li was lost from primary magmatic fluids during the retrograde skarn alteration. The fluid system in the Luziyuan deposit after the retrograde skarn alteration stage is Li-poor, and its Li isotopic signature is more susceptible to extraneous fluid.

The δ^7Li variation of the sulfide (sphalerite and galena) FIL overlaps the range of values from the actinolite FIL, which require additional

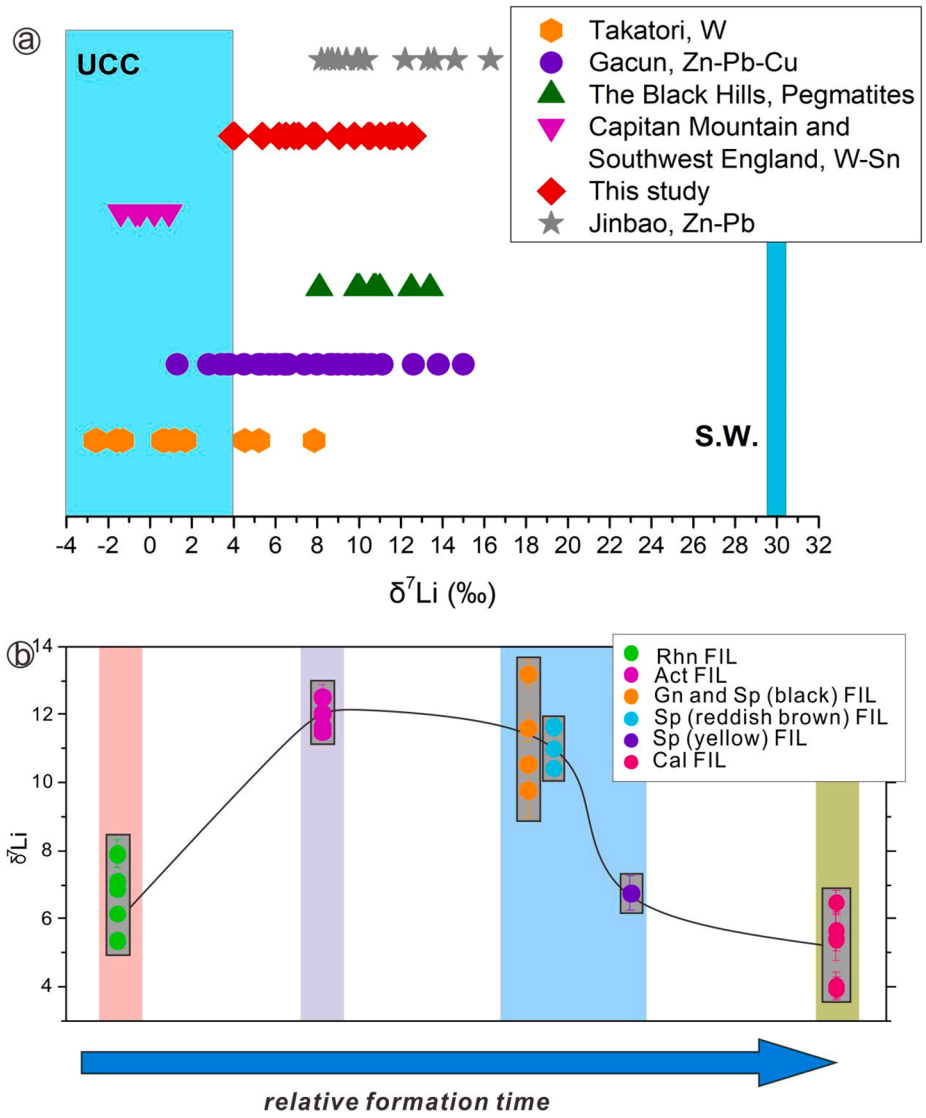

Fig. 6. (a) Comparison of the δ^7Li values of fluid inclusion leachates from a range of deposits. Data are from Teng et al. (2006), Masukawa et al. (2013), Yang et al. (2015), Richard et al. (2018), and Xu et al. (2018). UCC: upper continental crust; S.W.: seawater. (b) Evolution of the Li isotopic composition of ore-forming fluids at the Luziyuan deposit.

explanations (Table 1; Fig. 6. b). It is well established that fluid boiling and/or involvement of extraneous cool fluids are responsible for sulfide mineralization in skarn deposits (e.g., Meinert, 1987; Wilkinson, 2001; Samson et al., 2008; Palinkas et al., 2013). Previous studies showed that decompression-induced boiling involving vapor and liquid phase separation, is accompanied with a minor Li isotopic fractionation (<0.5‰), and isotopically heavy Li will preferentially enter the liquid phase (Foustoukos et al., 2004; Liebscher et al., 2007). Even though extreme Rayleigh fractionation occurs, Li isotopic signature of the residual liquid phase will not be altered by more than 1‰ within a boiling hydrothermal system (Liebscher et al., 2007). In addition, lithium is usually enriched in the brine-rich phase during boiling (Araoka et al., 2016). Hence, the residual fluids after boiling will have a lithium isotopic signature similar to or slightly heavier than the initial fluids. Therefore, fluid boiling explains the small differences in δ^7Li values amongst actinolite, galena, black sphalerite, and reddish-brown sphalerite FIL, and is consistent with fluid inclusion assemblages that record boiling (Deng et al., 2018).

However, this mechanism cannot account for sulfide FIL with low δ^7Li values, such as the light-yellow sphalerite FIL (+6.75‰, LZYNO11). The light-yellow sphalerite is considered to have precipitated from hydrothermal fluids following precipitation of the black and/or reddish-brown sphalerite. Moreover, calcite FIL that reflect the post-ore stage fluids contain the lowest δ^7Li value (+3.47‰) in all samples. Therefore, another reasonable explanation for the data is that extraneous fluids with isotopically light Li are involved into the hydrothermal system during the precipitation of light-yellow sphalerite. As depicted in Fig. 9, it is apparent that the light-yellow sphalerite FIL and calcite FIL suggest a good mixing trend of magmatic fluids with an extraneous fluid source. In addition, the H–O isotopes showed a slightly negative deviation trend from rhodonite fluid inclusions (fall into magmatic fluid) as compared to sphalerite fluid inclusions, suggesting a predominately meteoric origin in calcite fluid inclusions (Deng et al., 2018; Xu et al., 2019). Similarly, the lower δ^7Li values in fluids of meteoric origin have been documented recently in the Panasqueira W–Sn deposits (Richard et al., 2018). Therefore, we infer that hydrothermal mineralization at the Luziyuan deposit was triggered by the combined effects of the boiling of magmatic fluids and mixing with other fluids.

6.2. *Chlorine isotopes*

The two rhodonite samples (FIL-LZY-NO13-2 vs. LZY-NO30) display

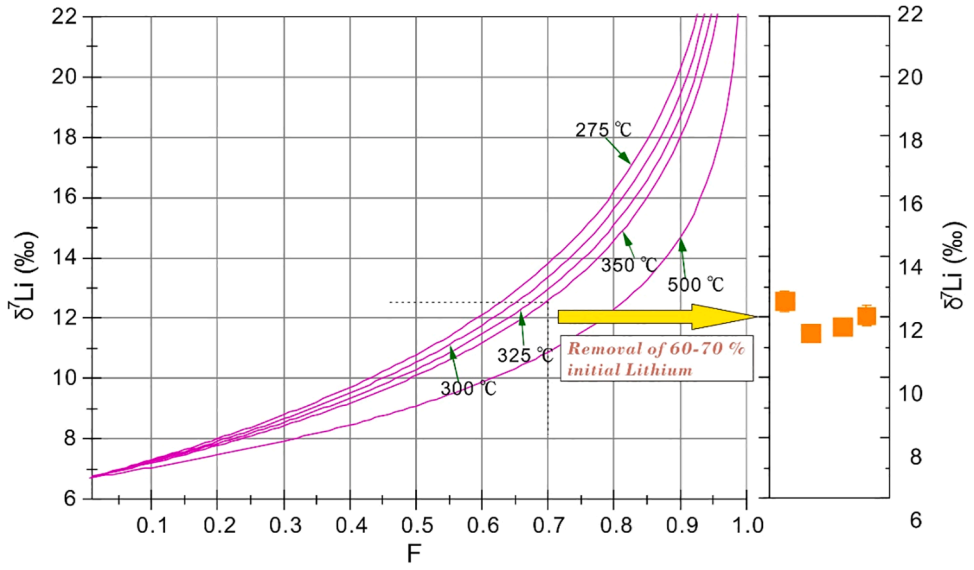

Fig. 7. Comparison of the calculated Rayleigh fractionation of Li isotopes during the retrograde skarn stage with the δ^7Li values of fluid inclusions.

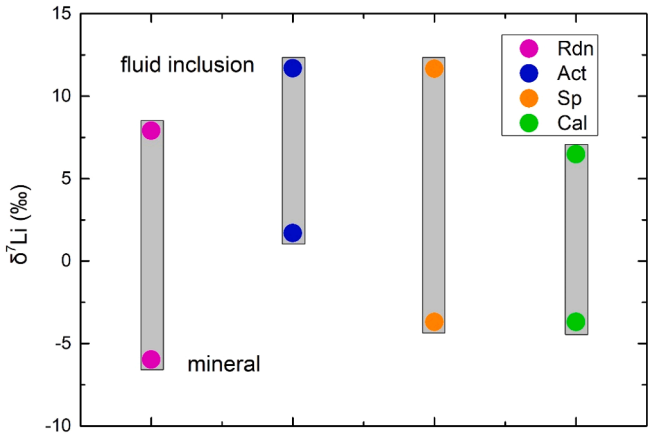

Fig. 8. δ^7Li values of co-existing minerals and fluid-inclusions.

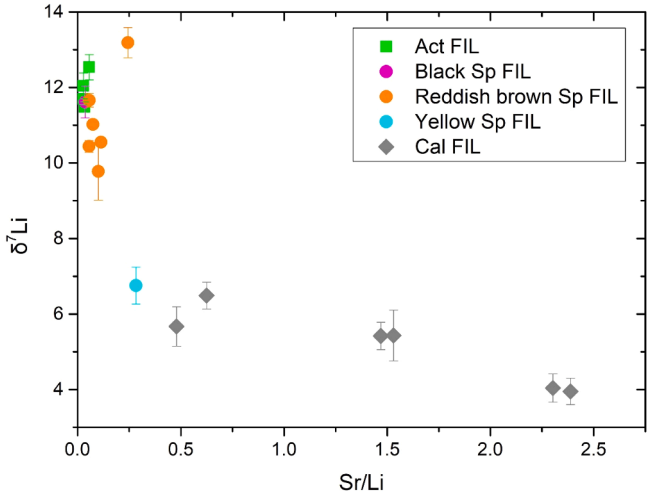

Fig. 9. δ^7Li values versus Sr/Li ratios for the fluid inclusion leachates.

δ^{37}Cl varying from +1.82‰ to +1.83‰ with an average value of +1.83‰. These positive δ^{37}Cl values are distinguishable from those of meteoric water and worldwide seawater, but are roughly comparable to the ranges seen in magmatic hydrothermal fluids (Banks et al., 2000a; Bernal et al., 2014, 2017; Gleeson and Smith, 2009; Richard et al., 2011; Andersson et al., 2019) (Fig. 10.). This excludes seawater or meteoric water as the origin of metallogenic fluids for most of the chlorides during the prograde skarn alteration stage. By contrast, magmatic chlorine reservoirs have a variable range of isotopic composition, from prominently negative values (−4.1‰) in porphyry copper deposits and iron oxide–copper–gold deposits, to positive values (+1.9‰) in the Sn–W mineralization associated with the Cornubian batholith in SW England (Nahnybida et al., 2009; Banks et al., 2000a). If ^{37}Cl-enriched biotite and apatite are taken into account (Andersson et al., 2019), the magmatic δ^{37}Cl values would be more positive. Cl isotopic composition of peraluminous medium–acid magma is still subject to in debate. Regardless of this debate, magma is expected to have extremely negative or positive values considering an inhomogeneous crust (Li et al., 2015), which agree with our data. Moreover, prograde metamorphism produces no discernible chlorine isotope fractionation (Selverstone and Sharp, 2015; Balan et al., 2019). Therefore, we conclude that the salinity in fluids found at the Luziyuan deposit is sourced from granite (Fig. 10).

However, it is apparent that the relatively lighter Cl isotopic composition occurs in FIL extracted from the later-formed actinolite. Kusebauch et al. (2015) reported fractionation of Cl isotopes during fluid–rock interaction within the Bamble Sector, SE Norway. They inferred that Rayleigh fractionation related to formation of Cl-rich silicate minerals caused a decrease in the δ^{37}Cl value of the fluid. Most of the Cl in the fluids was sequestered by amphibole during fluid–rock interaction, based on calculations assuming a mineral–fluid fractionation factor of 1.001. The Li and H–O isotopic compositions show that retrograde alteration at the Luziyuan deposit occurred within a closed system, satisfying the requirement for fluid evolution. According to the mentioned model, at least 70% Cl must be distilled from ore-forming fluids to offset the decreasing δ^{37}Cl values (Fig. 11). Consumption of Cl is attributable mostly to formation of hydrous minerals such as actinolite, chlorite, and biotite, and the formation of magnetite by reactions such as $FeCl_2 + 2\,H_2O = Fe(OH)_2 + 2HCl$ and $2\,Fe(OH)_2 + FeCl_2 = Fe_3O_4 + 2\,HCl + H_2$ during retrograde skarn alteration at the Luziyuan deposit. However, fluid:rock ratios (f/r) are high in hydrothermal ore-forming systems, much higher than the estimated f/r value of 1:1 calculated for the amphibolitization zone of Kusebauch et al. (2015).

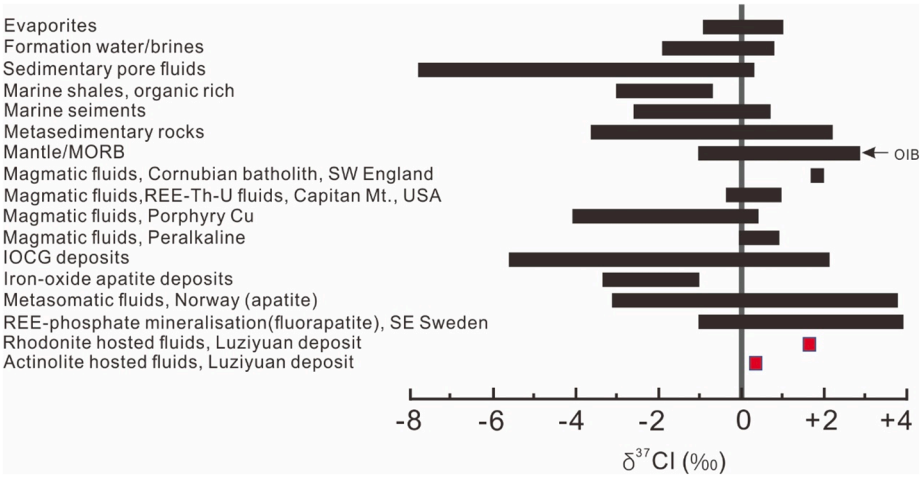

Fig. 10. Comparison of the $\delta^{37}Cl$ values of FIL with published values for a range of reservoirs (modified from Andersson et al., 2019).

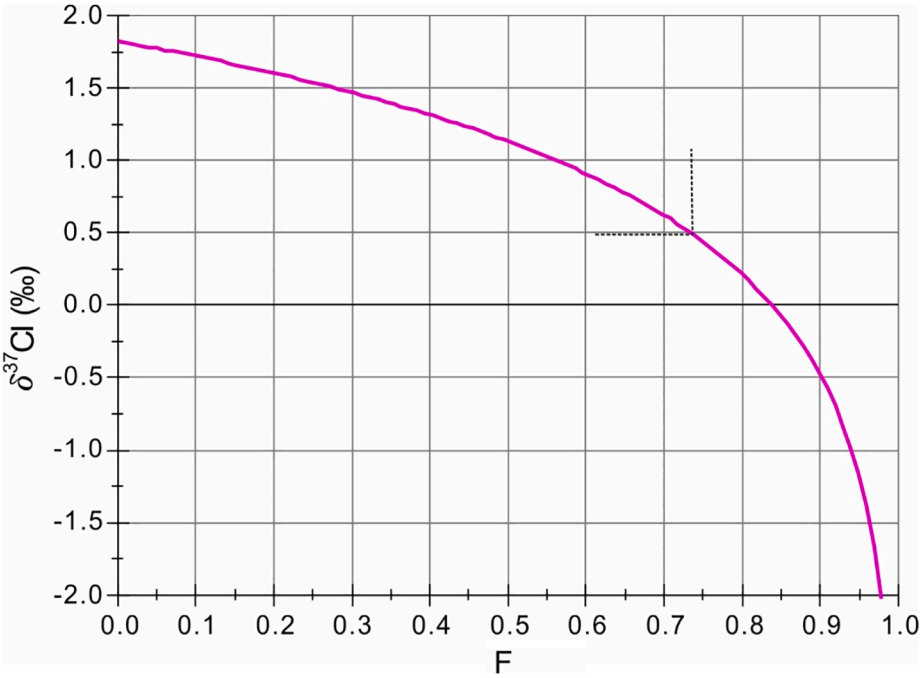

Fig. 11. Rayleigh fractionation of Cl isotopes during crystallization of Cl-bearing minerals.

Hence, the Cl consumption in the fluids could be negligible for the entire magmatic fluids that carry huge amounts of metals through Cl complexing ligand. Accordingly, we infer that the low $\delta^{37}Cl$ values of actinolite FIL are unlikely to reflect evolution of the ore-forming fluid during retrograde skarn alteration, and speculate that the Cl isotopic compositions of FIL from hydrous minerals do not reflect the origin of ore-forming fluids.

7. Conclusion

The elemental ratios and Li and Cl isotopic compositions are useful indicators of fluid sources and evolution. The fluid's geochemical characteristics provide new insights into the ore-forming process in the Luziyuan skarn Zn–Pb–Fe–(Cu) deposit, southwest of China. The Li and Cl isotopic compositions of rhodonite FIL suggest a magmatic source of the ore-forming fluids. However, such magmatic $\delta^{7}Li$ values of the hydrothermal fluids are not retained in actinolite FIL, and a significant fractionation occurs during the retrograde skarn stage. The formation of hydrous minerals extracts most Li from the ore-forming fluids with preferential loss of isotopically light Li. During the sulfide ore stage, fluid boiling and mixing with external and isotopically lighter Li fluids are the most crucial factors for the hydrothermal mineralization at the Luziyuan deposit. In addition, Cl isotopic compositions of hydrous mineral FIL could not efficiently identify the signature of fluid source. Nevertheless, our results show that non-traditional stable isotopes such as Li and Cl provide valuable insights into hydrothermal ore-forming systems.

Declaration of Competing Interest

The authors declare that they have no known competing financial interests or personal relationships that could have appeared to influence the work reported in this paper.

Acknowledgements

We wish to thank Ting Zhou, Yunqi Ma, Hongwen Lin, Peng Zhang, Xiuqun Yang and Yuhong Fan for their guidance and technical support for the chemical analysis. This project was financially supported by the discretionary foundation of the State Key Laboratory of Nuclear Resources and Environment (Z1913), DHBK2019314, the National Key R&D Programme of China (2017YFC0602500), Guizhou Scientific and Technological Innovation Team (2017-5657), National Natural Science Foundation of China (No. 41673024, 41363001).

Appendix A. Supplementary data

Supplementary data to this article can be found online at https://doi.org/10.1016/j.oregeorev.2021.104057.

References

Andersson, S.S., Wagner, T., Jonsson, E., Fusswinkel, T., Whitehouse, M.J., 2019. Apatite as a tracer of the source, chemistry and evolution of ore-forming fluids: The case of the Olserum-Djupedal REE-phosphate mineralisation, SE Sweden. Geochim. Cosmochim. Acta 255, 163–187.

Araoka, D., Nishio, Y., Gamo, T., Yamaoka, K., Kawahata, H., 2016. Lithium isotopic systematics of submarine vent fluids from arc and back-arc hydrothermal systems in the western Pacific. Geochem. Geophys. Geosyst. 17 (10), 3835–3853.

Balan, E., Créon, L., Sanloup, C., Aléon, J., Blanchard, M., Paulatto, L., Bureau, H., 2019. First-principles modeling of chlorine isotope fractionation between chloride-bearing molecules and minerals. Chem. Geol. 525, 424–434.

Banks, D.A., Boyce, A.J., Samson, I.M., 2002. Constraints on the origins of fluids forming Irish Zn-Pb-Ba deposits: Evidence from the composition of fluid inclusions. Econ. Geol. 97 (3), 471–480.

Banks, D.A., Gleeson, S.A., Green, R., 2000a. Determination of the origin of salinity in granite-related fluids: evidence from chlorine isotopes in fluid inclusions. J. Geochem. Explor. 69, 309–312.

Banks, D.A., Green, R., Cliff, R.A., Yardley, B.W.D., 2000b. Chlorine isotopes in fluid inclusions: determination of the origins of salinity in magmatic fluids. Geochim. Cosmochim. Acta 64 (10), 1785–1789.

Barnes, J.D., Cisneros, M., 2012. Mineralogical control on the chlorine isotope composition of altered oceanic crust. Chem. Geol. 326, 51–60.

Berger, G., Schott, J., Guy, C., 1988. Behavior of Li, Rb and Cs during basalt glass and olivine dissolution and chlorite, smectite and zeolite precipitation from seawater: experimental investigations and modelization between 50 and 300 °C. Chem. Geol. 71 (4), 297–312.

Bernal, N.F., Gleeson, S.A., Dean, A.S., Liu, X.M., Hoskin, P., 2014. The source of halogens in geothermal fluids from the taupo volcanic zone, north island, new zealand. Geochim. Cosmochim. Acta 126 (2), 265–283.

Bernal, N.F., Gleeson, S.A., Smith, M.P., Barnes, J.D., Pan, Y., 2017. Evidence of multiple halogen sources in scapolites from iron oxide-copper-gold (IOCG) deposits and regional NaCl metasomatic alteration, Norrbotten County, Sweden. Chem. Geol. 451, 90–103.

Brenan, J.M., Neroda, E., Lundstrom, C.C., Shaw, H.F., Ryerson, F.J., Phinney, D.L., 1998. Behaviour of boron, beryllium, and lithium during melting and crystallization: constraints from mineral-melt partitioning experiments. Geochim. Cosmochim. Acta 62 (12), 2129–2141.

Bryant, C.J., Chappell, B.W., Bennett, V.C., McCulloch, M.T., 2004. Lithium isotopic compositions of the New England Batholith: correlations with inferred source rock compositions. Trans. R. Soc. Edinb. Earth Sci, 95, 199-214.

Caciagli, N., Brenan, J.M., McDonough, W.F., Phinney, D., 2011. Mineral–fluid partitioning of lithium and implications for slab–mantle interaction. Chem. Geol. 280 (3–4), 384–398.

Chan, L.H., Edmond, J.M., Thompson, G., 1993. A lithium isotope study of hot-springs and metabasalts from mid-ocean ridge hydrothermal systems. J. Geophys. Res. 98, 9653–9656.

Chan, L.H., Joris, G., You, C.F., Edmond, J.M., 1994. Lithium isotope geochemistry of sediments and hydrothermal fluids of the guaymas basin, gulf of california. Geochim. Cosmochim. Acta 58 (20), 4443–4454.

Chan, L.H., Starinsky, A., Katz, A., 2002. The Behavior of Lithium and Its Isotopes in Oilfield Brines: Evidence from the Heletz-Kokhav Field. Israel. Geochimica et Cosmochimica Acta 66 (4), 615–623.

Chen, F., Deng, J., Shu, Q., Li, G., Cui, X., Zhao, F., Wang, Q., 2017. Geology, fluid inclusion and stable isotopes (O, S) of the Hetaoping distal skarn Zn-Pb deposit, northern Baoshan block, SW China. Ore Geol. Rev. 90, 913–927.

Deng, J., Wang, Q., Li, G., Santosh, M., 2014a. Cenozoic tectono-magmatic and metallogenic processes in the Sanjiang region, southwestern China. Earth Sci. Rev. 138, 268–299.

Deng, M.G., Chen, W., Wang, X.W., Liu, F.X., Guan, S.J., Lu, Y.X., Yu, H.J., Zhao, F., 2018. Fluid inclusion and ore genesis of the Luziyuan distal skarn Pb-Zn-Fe(-Cu) poly-metallic deposit, West Yunnan. SW China. Acta Petrologica Sinica 34 (5), 1239–1257 (in Chinese with English abstract).

Deng, M.G., Lin, B.X., Liang, X.W., Li, W.C., 2014b. Geological Characteristics of Rare Earths Elements and Its Indication Significance of Ore-Forming Fluid of Luziyuan Lead-Zinc Polymetallic Deposit in Yunnan. Journal of the Chinese Society of Rare Earths 31 (1), 117–128 (in Chinese with English abstract).

Deng, M.G., Xu, R., Wang, P., Sun, B.D., Zeng, L., Yu, H.J., Wang, T., Sha, J.Z., 2016. Geochemistry of the rhodonite in the Luziyuan Pb-Zn-Fe polymetallic deposit in West Yunnan and their genesis significance. Acta Petrologica Sinica 32 (8), 2248–2264 (in Chinese with English abstract).

Dong, M.L., Dong, G.C., Mo, X.X., Santosh, M., Zhu, D.C., Yu, J.C., Nie, F., Hu, Z.C., 2013. Zircon U-Pb geochronology Hf isotopes, and geochemistry of leucogranites in the Baoshan Block, western Yunnan: implications for Early Paleozoic arc magmatism along Gondwana margin. Lithos 179, 36–47.

Eastoe, C.J., Guilbert, J.M., Kaufmann, R.S., 1989. Preliminary evidence for fractionation of stable chlorine isotopes in ore-forming hydrothermal systems. Geology 17 (3), 285–288.

Fabbrizio, A., Stalder, R., Hametner, K., Günther, D., Marquardt, K., 2013. Experimental partitioning of halogens and other trace elements between olivine, pyroxenes, amphibole and aqueous fluid at 2 GPa and 900–1300 °C. Contrib. Miner. Petrol. 166 (2), 639–653.

Foustoukos, D.I., James, R.H., Berndt, M.E., Seyfried, W.E., 2004. Lithium Isotopic Systematics of Hydrothermal Vent Fluids at the Main Endeavour Field, Northern Juan De Fuca Ridge. Chem. Geol. 212 (1), 17–26.

Gleeson, S.A., Smith, M.P., 2009. The sources and evolution of mineralising fluids in iron oxide–copper–gold systems, Norrbotten, Sweden: Constraints from Br/Cl ratios and stable Cl isotopes of fluid inclusion leachates. Geochim. Cosmochim. Acta 73 (19), 5658–5672.

He, M.Y., Luo, C.G., Lu, H., Jin, Z.D., Deng, L., 2019. Measurements of lithium isotopic compositions in coal using MC-ICP-MS. J. Anal. At. Spectrom. 34 (9), 1773–1778.

Jahn, S., Wunder, B., 2009. Lithium speciation in aqueous fluids at high P and T studied by ab initio molecular dynamics and consequences for Li-isotope fractionation between minerals and fluids. Geochim. Cosmochim. Acta 73 (18), 5428–5434.

Kusebauch, C., John, T., Barnes, J.D., Klügel, A., Austrheim, H.O., 2015. Halogen element and stable chlorine isotope fractionation caused by fluid–rock interaction (Bamble Sector, SE Norway). J. Petrol. 56 (2), 299–324.

Li, L., Bonifacie, M., Aubaud, C., Crispi, O., Dessert, C., Agrinier, P., 2015. Chlorine isotopes of thermal springs in arc volcanoes for tracing shallow magmatic activity. Earth Planet. Sci. Lett. 413, 101–110.

Liebscher, A., Meixner, A., Romer, R.L., Heinrich, W., 2007. Experimental calibration of the vapour–liquid phase relations and lithium isotope fractionation in the system H_2O–LiCl at 400 °C/20–28 MPa. Geofluids 7 (3), 369–375.

Liu, S., Hu, R.Z., Gao, S., Feng, C.X., Huang, Z., Lai, S., Yuan, H., Liu, X., Coulson, I.M., Feng, G., 2009. U-Pb zircon, geochemical and Sr–Nd–Hf isotopic constraints on the age and origin of Early Palaeozoic I-type granite from the Tengchong-Baoshan Block, Western Yunnan Province, SW China. J. Asian Earth Sci. 36 (2–3), 168–182.

Liu, W., Deng, M.G., 2014. A study of mineral characteristics and metallogenic stages of Luziyuan Pb-Zn-Fe polymetallic ore deposit, Zhenkang in Yunnan Province. Contribution to Geology and Mineral Resources Research 29 (3), 381–386 (in Chinese with English abstract).

Luo, C.G., Xiao, Y.K., Ma, H.Z., Ma, Y.Q., Zhang, Y.L., He, M.Y., 2012. Stable isotope fractionation of chlorine during evaporation of brine from a saline lake. Chin. Sci. Bull. 57 (15), 1833–1843.

Luo, C.G., Xiao, Y.K., Wen, H.J., Ma, H.Z., Ma, Y.Q., Zhang, Y.L., He, M.Y., 2014. Stable isotope fractionation of chlorine during the precipitation of single chloride minerals. Appl. Geochem. 47, 141–149.

Magna, T., Janoušek, V., Kohút, M., Oberli, F., Wiechert, U., 2010. Fingerprinting sources of orogenic plutonic rocks from Variscan belt with lithium isotopes and possible link to subduction-related origin of some A-type granites. Chem. Geol. 274 (1), 94–107.

Magna, T., Novák, M., Cempírek, J., Janoušek, V., Ullmann, C.V., Wiechert, U., 2016. Crystallographic control on lithium isotope fractionation in Archean to Cenozoic lithium-cesium-tantalum pegmatites. Geology 44 (8), 655–658.

Marschall, H.R., Pogge, V.S.P.A.E., Seitz, H.M., Elliott, T., Niu, Y., 2007. The lithium isotopic composition of orogenic eclogites and deep subducted slabs. Earth Planet. Sci. Lett. 262 (3), 563–580.

Masukawa, K., Nishio, Y., Ken-Ichiro, H., 2013. Lithium-strontium isotope and heavy metal content of fluid inclusions and origin of ore-forming fluid responsible for tungsten mineralization at Takatori mine. Japan. Geochemical Journal 47 (3), 309–319.

Meinert, L.D., 1987. Skarn zonation and fluid evolution in the Groundhog mine, Central mining district. New Mexico. Economic Geology 82 (3), 523–545.

Meinert, L.D., Dipple, G.M., Nicolescu, S., 2005. World Skarn Deposits: Economic Geology 100th Anniversary Volume. pp. 299-336.

Millot, R., Petelet-Giraud, E., Guerrot, C., Négrel, P., 2010a. Multi-isotopic composition (δ^7Li–δ^{11}B–δD–δ^{18}O) of rainwaters in France: Origin and spatio-temporal characterization. Appl. Geochem. 25 (10), 1510–1524.

Millot, R., Vigier, N., Gaillardet, J., 2010b. Behaviour of lithium and its isotopes during weathering in the Mackenzie Basin. Canada. Geochimica et Cosmochimica Acta 74 (14), 3897–3912.

Nahnybida, T., Gleeson, S.A., Rusk, B.G., Wassenaar, L.I., 2009. Cl/Br ratios and stable chlorine isotope analysis of magmatic–hydrothermal fluid inclusions from Butte, Montana and Bingham Canyon. Utah. Mineralium Deposita 44 (8), 837.

Palinkas, S.S., Palinkas, L.A., Renac, C., Spangenberg, J.E., Luders, V., Molnar, F., Mallqi, G., 2013. Metallogenic Model of the Trepca Pb-Zn-Ag Skarn Deposit, Kosovo: Evidence from Fluid Inclusions, Rare Earth Elements, and Stable Isotope Data. Econ. Geol. 108 (1), 135–162.

Richard, A., Banks, D.A., Hendrikssona, N., Lahaye, N., 2018. Lithium isotopes in fluid inclusions as tracers of crustal fluids: An exploratory study. Lithium isotopes in fluid inclusions as tracers of crustal fluids: An exploratory study. J. Geochem. Explor. 184, 158–166.

Richard, A., Banks, D.A., Mercadier, J., Boiron, M.C., Cuney, M., Cathelineau, M., 2011. An evaporated seawater origin for the ore-forming brines in unconformity-related uranium deposits (Athabasca Basin, Canada): Cl/Br and δ^{37}Cl analysis of fluid inclusions. Geochim. Cosmochim. Acta 75 (10), 2792–2810.

Romer, R.L., Meixner, A., 2014. Lithium and boron isotopic fractionation in sedimentary rocks during metamorphism-the role of rock composition and protolith mineralogy. Geochim. Cosmochim. Acta 128 (3), 158–177.

Samson, I.M., Williams-Jones, A.E., Ault, K.M., Gagnon, J.E., Fryer, B.J., 2008. Source of fluids forming distal Zn-Pb-Ag skarns: Evidence from laser ablation–inductively coupled plasma–mass spectrometry analysis of fluid inclusions from El Mochito. Honduras. Geology 36 (12), 947–950.

Selverstone, J., Sharp, Z.D., 2015. Chlorine isotope behavior during prograde metamorphism of sedimentary rocks. Earth Planet. Sci. Lett. 417, 120–131.

Shannon, R.D., 1976. Revised effective ionic radii and systematic studies of interatomic distances in halides and chalcogenides. Acta crystallographica section A: crystal physics, diffraction, theoretical and general Crystallography 32 (5), 751–767.

Shu, Q., Chang, Z., Hammerli, J., Lai, Y., Huizenga, J.M., 2017. Composition and evolution of fluids forming the baiyinnuo'er Zn-Pb skarn deposit, northeastern china: insights from laser ablation icp-ms study of fluid inclusions. Econ. Geol. 112, 1441–1460.

Sone, M., Metcalfe, I., 2008. Parallel Tethyan sutures in mainland Southeast Asia: new insights for Palaeo-Tethys closure and implications for the Indosinian orogeny. C.R. Geosci. 340 (2–3), 166–179.

Tao, Y., Hu, R.Z., Zhu, F.L., Ma, Y.S., Ye, L., Cheng, Z.T., 2010. Ore-forming age and the geodynamic background of the Hetaoping Lead-zinc deposit in Baoshan. Yunnan. Acta Petrologica Sinica 26 (6), 1760–1772 (in Chinese with English abstract).

Teng, F.Z., McDonough, W., Rudnick, R., Dalpé, C., Tomascak, P., Chappell, B., Gao, S., 2004. Lithium isotopic composition and concentration of the upper continental crust. Geochim. Cosmochim. Acta 68 (20), 4167–4178.

Teng, F.Z., McDonough, W.F., Rudnick, R.L., Walker, R.J., Sirbescu, M.C., 2006. Lithium Isotopic Systematics of Granites and Pegmatites from the Black Hills. South Dakota. American Mineralogist 91 (10), 1488–1498.

Teng, F.Z., Rudnick, R.L., McDonough, W.F., Gao, S., Tomascak, P.B., Liu, Y., 2008. Lithium isotopic composition and concentration of the deep continental crust. Chem. Geol. 255 (1–2), 47–59.

Teng, F.Z., Rudnick, R.L., McDonough, W.F., Wu, F.Y., 2009. Lithium Isotopic Systematics of A-Type Granites and Their Mafic Enclaves: Further Constraints on the Li Isotopic Composition of the Continental Crust. Chem. Geol. 262 (3), 370–379.

Tian, S.H., Yang, Z.S., Hou, Z.Q., Mo, X.X., Hu, W.J., Zhao, Y., Zhao, X.Y., 2017. Subduction of the Indian lower crust beneath southern Tibet revealed by the post-collisional potassic and ultrapotassic rocks in SW Tibet. Gondwana Res. 41, 29–50.

Tomascak, P.B., Carlson, R.W., Shirey, S.B., 1999. Accurate and Precise Determination of Li Isotopic Compositions by Multi-Collector Sector Icp-Ms. Chem. Geol. 158 (1–2), 145–154.

Vezzoni, S., Dini, A., Rocchi, S., 2016. Reverse telescoping in a distal skarn system (Campiglia Marittima, Italy). Ore Geol. Rev. 77, 176–193.

Wang, D., Romer, R.L., Guo, J.H., Glodny, J., 2019. Li and B isotopic fingerprint of Archean subduction. Geochimica et Cosmochim. Acta, 268, 446-366.

Webster, J.D., Holloway, J.R., Hervig, R.L., 1989. Partitioning of lithophile trace elements between H_2O and H_2O+CO_2 fluids and topaz rhyolite melt. Econ. Geol. 84 (1), 116–134.

Wenger, M., Armbruster, T., 1991. Crystal chemistry of lithium: oxygen coordination and bonding. Eur. J. Mineral. 387–400.

Wilkinson, J.J., 2001. Fluid inclusions in hydrothermal ore deposits. Lithos 55 (1–4), 229–272.

Wood, S.A., Samson, I.M., 1998. Solubility of ore minerals and complexation of ore metals in hydrothermal solutions. Reviews in Economic Geology 10, 33–80.

Wunder, B., Deschamps, F., Watenphul, A., Guillot, S., Meixner, A., Romer, R.L., Wirth, R., 2010. The effect of chrysotile nanotubes on the serpentine-fluid li-isotopic fractionation. Contrib. Miner. Petrol. 159 (6), 781–790.

Wunder, B., Meixner, A., Romer, R.L., Feenstra, A., Schettler, C., Heinrich, W., 2007. Lithium isotope fractionation between Li-bearing staurolite, Li-mica and aqueous fluids: An experimental study. Chem. Geol. 238 (3), 277–290.

Wunder, B., Meixner, A., Romer, R. L, Heinrich, W., et al., 2006. Temperature-dependent isotopic fractionation of lithium between clinopyroxene and high-pressure fluids. Contrib. Mineral. Petrol. 151 (1), 112–120.

Xia, Q.L., Chen, Y.Q., Lu, Y.X., Jiang, C.X., Liu, H.G., Lü, Z.C., 2005. Geochemistry, fluid inclusion, and stable isotope studies of Luziyuan Pb-Zn deposit in Yunnan Province, southwestern China. Earth Sci. 30, 177–186 (In chinese with English abstract).

Xu, L., Luo, C.G., Wen, H.J., 2020a. A Revisited Purification of Li for "Na Breakthrough" and its Isotopic Determination by MC-ICP-MS. Geostand. Geoanal. Res. 44, 201–214.

Xu, L., Luo, C.G., Wen, H.J., Zhou, Z.B., Qing, C.J., 2018. Origin of ore-forming fluids of the Zn-Pb-(Cu) deposits in the Jinbao mine district of eastern Guizhou Province, China: Evidence from Chemical Compositions of Fluid Inclusions and their Lithium Isotopes. Geochem. J. 52 (6), 483–496.

Xu, R., Deng, M.G., Li, W.C., Lai, C.K., Zaw, K., Gao, Z.W., Chen, Y.H., Niu, C.H., Liang, G., 2020b. Origin of the giant Luziyuan Zn-Pb-Fe (-Cu) distal skarn deposit, Baoshan block, SE Tibet: Constraints from Pb–Sr isotopes, calcite C-O isotopes, trace elements and Sm–Nd dating. J. Asian Earth Sci. 205, 104587.

Xu, R., Li, W.C., Deng, M.G., Zhou, J.X., Ren, T., Yu, H.J., 2019. Genesis of the superlarge Luziyuan Zn-Pb-Fe (-Cu) distal skarn deposit in western Yunnan (SW China): Insights from ore geology and CHOS isotopes. Ore Geol. Rev. 107, 944–959.

Yang, D., Hou, Z.Z., Zhao, Y., Hou, K.J., Yang, Z.M., Tian, S.H., Fu, Q., 2015. Lithium Isotope Traces Magmatic Fluid in a Seafloor Hydrothermal System. Sci. Rep. 5 (3), 969–1006.

Yang, Q.J., Xu, Y.G., Huang, X.L., Luo, Z.Y., 2006. Geochronology and geochemistry of granites in the Gaoligong tectonic belt, western Yunnan: implications. Acta Petrologica Sinica 22 (4), 817–834 (In chinese with English abstract).

Yang, X.F., Luo, G., 2011. A tentative analysis of the ore-controlling factors of the Luziyuan lead-zinc deposit in Zhenkang area. Yunnan. Geological Bulletin of China 30 (7), 1137–1146 (In Chinese with English abstract).

Yang, X.J., Jia, X.C., Xiong, C.L., Bai, X.Z., Huang, B.X., Luo, G., Yang, C.B., 2012. LA-ICP-MS zircon U-Pb age of metamorphic basic volcanic rock in Gongyanghe Group of southern Gaoligong Mountain, western Yunnan Province, and its geological significance. Geological Bulletin of China 31 (2/3), 264–276 (In chinese with English abstract).

Yardley, B.W., 2005. metal concentrations in crustal fluids and their relationship to ore formation. Econ. Geol. 100 (4), 613–632.

YGS, 2012. The Exploration Verification Report of the Luziyuan Pb-Zn-Fe polymetallic Deposit, Zhenkang County, Yunnan Province. Unpubl. Rep 1–274.

Zack, T., Tomascak, P.B., Rudnick, R.L., Dalpe, C., McDonough, W.F., 2003. Extremely light Li in orogenic eclogites: The role of isotope fractionation during dehydration in subducted oceanic crust. Earth Planet. Sci. Lett. 208, 279–290.

Zeng, L., Deng, M.G., Yin, G.H., Wang, P., 2014. Characteristics and mineralization epochs of Skarn minerals of Luziyuan Pb-Zn deposit in ZhenKang, western Yunnan. Mineral Resources and Geology 28 (3), 286–292.